FISEVIER

Contents lists available at ScienceDirect

Applied Catalysis B: Environmental

journal homepage: www.elsevier.com/locate/apcatb



Looking at the overlooked hole oxidation: Photocatalytic transformation of organic contaminants on graphitic carbon nitride under visible light irradiation



Qinmin Zheng^a, Enshi Xu^{a,b}, Eun Park^b, Hanning Chen^b, Danmeng Shuai^{a,*,1}

- ^a Department of Civil and Environmental Engineering, The George Washington University, Washington, D.C., 20052, United States
- ^b Department of Chemistry, The George Washington University, Washington, D.C. 20052, United States

ARTICLE INFO

Keywords: Photocatalysis Graphitic carbon nitride Hole oxidation Binding energy Concerted proton-coupled electron transfer (CPCET)

ABSTRACT

Solar-energy-enabled photocatalysis is a sustainable process to destruct persistent environmental pollutants via the attack of photogenerated reactive species (e.g., holes, reactive oxygen species such as 'OH, O2 - /HO2', H₂O₂, and ¹O₂). Graphitic carbon nitride (g-C₃N₄) has emerged as a promising polymeric photocatalyst, and its highly tunable properties allow the material with an enhanced photocatalytic activity for environmental remediation. In this study, by taking advantage of simulation and experimental tools, we systematically evaluated the production of reactive species of undoped and carbon (C)-doped g-C₃N₄ samples, and identify the role of these species in contaminant oxidation under simulated visible sunlight irradiation (xenon lamp, $\lambda > 400$ nm). Both g-C₃N₄ samples produced negligible OH or triplet-excited states (³g-C₃N₄*), but the C-doped g-C₃N₄ sample generated more 1O2, O2-, and H2O2 compared to the undoped counterpart. Surprisingly, all these oxidative species did not contribute substantially for the degradation kinetics of contaminant phenol and atrazine, at least for the initial oxidation of the parent compounds; and the results otherwise highlighted the important role of the holes for contaminant transformation. The surface-mediated hole oxidation of the contaminants, including the adsorption of the contaminants on the photocatalyst surface (quantified by the binding free energy) and electron transfer kinetics from the contaminants to the excited photocatalysts (quantified by the concerted proton-coupled electron transfer (CPCET) rate) were investigated by molecular dynamics (MD) and density functional theory (DFT) simulations. The simulation results indicated that C-doping could favor the binding of atrazine but not of phenol on g-C₃N₄. The C-doping also significantly decreased the CPCET rate of phenol on g-C₃N₄ but could have little to no adverse impact for the CPCET rate of atrazine. These simulation and experimental results could explain the selective oxidation of phenol and atrazine on undoped and C-doped g- C_3N_4 in our previous study, and the results also highlight the dominant role of the holes for contaminant transformation that was largely overlooked before. This study generates mechanistic insights of photocatalytic oxidation, and will provide guidelines for the rational design of g-C₃N₄ as an effective visible-light-responsive photocatalyst for many applications, including contaminant degradation, chemical synthesis, and beyond.

1. Introduction

Photocatalysis is a promising technology for degrading organic contaminants in water, because the process can activate dissolved O_2 and/or H_2O to generate reactive oxygen species (ROS, e.g., ·OH, O_2^- ·/ HO_2 ·, 1O_2 , H_2O_2) and holes (h^+ , also known as electron vacancies) to attack contaminants under ambient conditions, and the process can potentially utilize renewable solar energy and promote sustainable water purification by reducing the energy and chemical consumption

[1–4]. Graphitic carbon nitride (g- C_3N_4) has attracted great attention for photocatalysis since 2009 [2], and the material has a number of merits to promote its application for water purification: (i) tunable band gaps of $1.5-2.7\,\mathrm{eV}$ that allow harvesting low-energy visible photons of $460-827\,\mathrm{nm}$, (ii) fabrication from earth-abundant and inexpensive precursors, and (iii) chemical stability and biocompatibility [5–13]. However, to date, one main limitation of g- C_3N_4 for photocatalytic water purification is its unknown reaction mechanism with the organic contaminants in water [14]. In contrast to most conventional

^{*} Corresponding author.

E-mail address: danmengshuai@gwu.edu (D. Shuai).

¹ Website: http://materwatersus.weebly.com/.

UV-light-responsive photocatalysts (e.g. TiO_2 , ZnO) [4,15] that predominantly generate ·OH, the most powerful oxidant in water [16], for organic contaminant oxidation, most g- C_3N_4 samples generate limited ·OH because the valence band edge of g- C_3N_4 (\sim 1.7 eV) is less positive than the reduction potential of ·OH/ H_2O ($E^\circ=2.32\,V$ at pH 7), thus prohibiting direct hole oxidation of H_2O at the valence band [12]. A series of other reactive species (e.g., ROS generated via the reduction of O_2 , holes) are believed to play a dominant role for degrading organic contaminants by g- C_3N_4 [14]. Therefore, a systemic evaluation of how the reactive species contribute to organic contaminant degradation on g- C_3N_4 should be conducted to understand material-contaminant interactions and to elucidate the mechanisms of contaminant removal.

ROS identification, quantification, and interactions with contaminants in a photocatalytic system have been successfully conducted in previous studies [17,18]. Particularly, g-C₃N₄ can be excited to triplet states by harvesting photons because of its polymeric nature [19,20], in contrast to many other photocatalysts. The triplet-excited states (3g-C3N4*) may also lead to contaminant degradation via electron or energy transfer [21,22], similar to natural chromophores (e.g., natural organic matter) in photolysis. Nevertheless, no study has investigated the production of ³g-C₃N₄* and its contribution to contaminant degradation in photocatalysis. Moreover, the characterization of photogenerated holes, especially hole-contaminant reaction mechanisms, was largely overlooked. Experimental evaluation of hole oxidation in an aqueous environment is challenging because both contaminant adsorption to the photocatalyst surface and electron transfer from the adsorbed contaminant to the photocatalyst are involved, and they are difficult to deconvolute. To date, the quenching experiment is the most widely-used method for evaluating hole generation and the contribution of the holes to contaminant degradation (e.g., with the addition of formic acid in photocatalysis to quench holes [23]), but the hole scavengers could also react with ROS and lead to artifacts in characterization. Some pioneer studies have evaluated hole oxidation for TiO2-based photocatalysis, including highly sensitive femtosecond and nanosecond transient absorption spectroscopy, electron paramagnetic resonance (EPR), and quantitative single-molecule, single-particle fluorescence imaging [24-26]. However, the sample preparation and experimental setup of these studies were complicated.

In our previous work, we observed selective contaminant degradation for phenol and atrazine on undoped and carbon (C)-doped g-C₃N₄ samples (i.e., U and MCB_{0.07}, respectively): C-doped g-C₃N₄ was 1.8 times more reactive for the degradation of atrazine than phenol, however, undoped g-C₃N₄ was 3.9 times more reactive for the degradation of phenol than atrazine under the same experimental condition (Table S1) [13]. In this study, we aim to understand the mechanism of selective contaminant degradation by comprehensively characterizing contaminant-photocatalyst interactions. We first evaluated ROS generation and their contribution to contaminant degradation. In addition, ³g-C₃N₄* that could also degrade the contaminants was quantified. Surprisingly, the results showed that holes, rather than ROS and ³g-C₃N₄*, played a dominant role in contaminant degradation. Next we applied molecular dynamics (MD) and density functional theory (DFT) simulations to investigate the whole process of hole oxidation, including contaminant adsorption and direct electron transfer kinetics to the excited photocatalyst [27,28]. Our study elucidated the mechanism of contaminant degradation on visible-light-responsive photocatalyst g-C₃N₄ by the synergy of simulation and experimental approaches, and highlighted the critical role of holes for oxidation for the first time. Hole oxidation could enhance the selectivity of photocatalysis via rational material design, which can greatly benefit contaminant removal in complex water matrices, chemical production with enhanced selectivity, and beyond.

2. Experimental section

Details of synthesis, characterization, reaction kinetics of the

undoped and C-doped g- C_3N_4 were included in our previous publication [13]. A summary of material synthesis is presented in the supporting information (SI).

2.1. Quantification of ROS and triplet-excited states of g-C₃N₄

Para-chlorobenzoic acid (p-CBA) is a well-known probe to detect ·OH due to its high reactivity with ·OH ($k = 5.2 \times 10^9 \text{ M}^{-1} \text{ s}^{-1}$) [29–31]. FFA is extremely reactive toward $^{1}O_{2}$ ($k = 1.2 \times 10^{8} \text{ M}^{-1}$ s⁻¹) and adequately specific for ${}^{1}O_{2}$ detection [20,32]. The decay of p-CBA and FFA was analyzed by high performance liquid chromatography (HPLC) to determine the steady-state concentration of ·OH and ¹O₂ in photocatalysis, respectively. The steady-state concentration of ·O₂ - in photocatalysis was quantitatively analyzed by detecting the reduction of XTT (2, 3-bis (2-methoxy-4-nitro-5-sulfophenyl)-2H-tetrazolium-5-carboxanilide) and the formation of XTT -- with a UV-vis spectrophotometer [31,33]. The accumulated concentration of H₂O₂ in photocatalysis was measured colorimetrically by the DPD method [34]. The steady-state concentration of ³g-C₃N₄* was determined by monitoring the formation of four isomers of trans, trans-hexadienoic acid (HAD) as probes using HPLC [35]. Details of these methods are presented in the SI.

2.2. Simulated binding free energy of contaminants on g-C₃N₄ sheets

The reaction coordinate of the contaminant-sheet binding is first defined as the distance, R_{cs} , between their centers of mass (COM) along the surface normal of the sheet. Then, the umbrella sampling technique [36] was employed to constraint R_{cs} at various values from 2.0 to 9.0 Å with a force constant of 1.0 kcal $\text{mol}^{-1} \text{ Å}^{-2}$. Finally, the binding free energy profile was reconstructed from the biased samples of R_{cs} using the weighted histogram analysis method (WHAM) [37]. More specifically, both the contaminant and the g-C₃N₄ sheet were described by the generalized Amber force field (GAFF) [38], while their aqueous solvents were represented by a flexible simple point-charge (SPC/Fw) water model [39]. In each of the 32 umbrella sampling windows, a 1.0ns production MD trajectory with a time step of 1.0 fs was obtained after the system had been equilibrated for 0.5 ns under a Nose-Hoover thermostat [40,41] at 298 K. Unless otherwise specified, all of our calculations were performed by CP2K [42], an open-source molecular simulation package.

2.3. Simulated rate of concerted proton-coupled electron transfer (CPCET) from contaminants to photo-excited g- C_3N_4 sheets

The proton-coupled electron transfer in our contaminant/g-C₃N₄ adducts is a concerted bidirectional process wherein the oxidation of a contaminant is simultaneously accompanied by its loss of a proton to the photo-excited g-C₃N₄ sheet. Given the strikingly unstable intermediates if the reaction follows the sequential mechanism (i.e., proton transfer \rightarrow electron transfer, or electron transfer \rightarrow proton transfer), we only considered the nonadiabatic transitions directly between the reactant and product electron-proton vibronic states in our simulations. Analogous to Marcus theory [43], a CPCET reaction is along a collective solvent coordinate, which encodes the reorganization of the solvent environment, the fundamental driving force for a non-radiative transition like CPCET. In this regard, the rate of CPCET can be readily derived from the Fermi's Golden rule [44] by exploring all possible pairs of reactant and product vibronic states. Under a short-time approximation for fast solvent dynamics, the distribution of all vibronic states follows the Bose-Einstein statistics, leading to a closed form of CPCET rate [45] as will be thoroughly discussed in the results and discussion.

3. Results and discussion

3.1. Quantification of ROS and ${}^{3}g$ - $C_{3}N_{4}$ * in photocatalysis

ROS production was quantified by employing radical probes that are selective and fast to react with specific radicals (details in the SI) under the same experimental conditions for contaminant degradation (pH 7.3, visible light irradiation (xenon lamp, 1000 W, $\lambda > 400$ nm)). In our system, no measurable degradation of p-CBA, a probe for ·OH, was observed over the experimental time scale. It indicated that negligible ·OH was generated for both undoped and C-doped g-C₃N₄ (under the detection limit, $< 10^{-15}$ M, see the SI) [46], which is likely due to the less positive valence band of g-C₃N₄ that inhibits ·OH production via the hole oxidation of H2O. The decay of FFA confirmed the generation of ¹O₂ in our system, and C-doped g-C₃N₄ produced 2.0-fold of ¹O₂ than undoped g-C₃N₄ (4.69 \pm 2.00 \times 10⁻¹² vs. 2.37 \pm 0.29 \times 10⁻¹² M). O2-has also been detected based on the reduction of XTT, and the result showed that C-doped g-C₃N₄ generated 2.4-fold of O₂ - · than undoped g-C₃N₄ (9.64 \pm 3.39 \times 10⁻¹² vs. 3.95 \pm 0.61 \times 10⁻¹² M). Compared to $O_2 - \cdot$, the concentration of hydroperoxyl radical (HO₂·) was negligible under our test conditions (pKa = 4.8 vs. reaction solution pH of 7.3) [47]. Both g-C₃N₄ generated comparable concentration of H₂O₂ (i.e., 2-4 µM in 1-6 h experiment, Fig. S1), which was measured by the DPD method [34]. The results of ROS production of undoped and C-doped g-C₃N₄ are summarized in Table 1.

In addition to ROS, ${}^3g\text{-}C_3N_4{}^*$ was observed since it could also contribute to contaminant degradation via electron or energy transfer [21,22]. Sorbic acid (triplet energy $E_T=249\,\mathrm{kJ}$ mol $^{-1}$) was used to measure high-energy ${}^3g\text{-}C_3N_4{}^*$ [35], however, we did not detect the production of high-energy ${}^3g\text{-}C_3N_4{}^*$ (under the detection limit, $<10^{-16}$ M) [48]. Low-energy ${}^3g\text{-}C_3N_4{}^*$ reacts with 3O_2 readily to form 1O_2 because of the low E_T of 1O_2 (94 kJ mol $^{-1}$) [22], and the concentration of 1O_2 has already been quantified. The results of ${}^3g\text{-}C_3N_4{}^*$ production of undoped and C-doped $g\text{-}C_3N_4$ are also summarized in Table 1.

3.2. Evaluation of reactive species contribution to contaminant degradation

To understand the contribution of all reactive species (i.e., ROS, 3g C $_3N_4*$, and holes) to contaminant degradation, we compared the observed contaminant degradation rate constant ($k_{\rm obs}$) in our previous study (details in Table 1) [13] with the calculated contaminant degradation rate constant (k) in this study. k is the summation of the first-order reaction rate constant of each reactive species for contaminant

degradation:

$$k = k_{\text{OH}} [\cdot \text{OH}]_{SS} + k_{1_{O_2}} [^1 \text{O}_2]_{SS} + k_{0_2^-} [O_2^- \cdot]_{SS} + k_{3_{g-C_3N_4*}} [^3 g - C_3 N_4^*]_{SS}$$

$$+ k_{H_2O_2} [H_2 \text{O}_2]_{SS} + k_{h^+} [h^+]_{SS}$$
(1)

where $k_{\cdot OH}$, $k_{^1O_2}$, $k_{O_2^-}$, $k_{^3g-C_3N_4*}$, $k_{H_2O_2}$, and k_{h^+} are the second-order reaction rate constants of contaminant reactions with the reactive species, and $[\cdot OH]_{ss}$, $[^{1}O_{2}]_{ss}$, $[O_{2}^{-\bullet}]_{ss}$, $[^{3}g-C_{3}N_{4}^{*}]_{ss}$, $[H_{2}O_{2}]_{ss}$, and $[h^{+}]_{ss}$ are the steady-state concentration of the reactive species. A summary of the available second-order reaction rate constants is tabulated in Table 1. The reaction rate constants of atrazine and phenol with 'OH and ¹O₂ are well-documented [48,49]. H₂O₂ could not react with either atrazine or phenol under visible light irradiation ($\lambda > 400 \text{ nm}$) based on our control experiments. Therefore, the contribution of H2O2 for contaminant degradation can be neglected. The reaction rate constant of phenol and O_2^- is known [50], but not for atrazine and O_2^- . Atrazine contains a couple of functional groups or moieties that could react with O_2^- , e.g., chlorine, amine, and O_2^- may lead to dechlorination via nucleophilic substitution [51] or proton abstraction of the amine. Several reaction kinetics have been reported for chlorinated aromatic compounds or amines with $O_2^{-}\cdot$, and the second-order reaction rate constants are within the order of 10³ M⁻¹ s⁻¹ [52]. Therefore, it is reasonable for us to assume the second-order reaction rate constant of atrazine and O_2^- is in the same range. In addition, no reaction rate constant was reported for ³g-C₃N₄* with the contaminants. We used the reaction rate constants between the contaminants and triplet-excited state dissolved organic matter (3 DOM*) to approximate $k_{^3g-C_3N_4*}$ [48,53]. There is very few study to quantify hole generation and study the second-order reaction rate constant between the holes and the contaminants, possibly because the process involves complex multiple interactions (e.g., photon excitation, contaminant adsorption, hole oxidation, hole migration, charge recombination) and the reduction potential of holes are not well-characterized. Therefore, the steady-state concentration of the holes and hole-contaminant reaction rate constants are not known to date.

We summed up the contribution of all ROS and 3 g-C₃N₄* for contaminant degradation (in the order of 10^{-6} - 10^{-5} s⁻¹), and surprisingly observed that these reactive species did not contribute substantially to contaminant removal (k_{obs} in the order of 10^{-4} s⁻¹). The results highlight that hole oxidation played a dominant role in contaminant degradation, at least for initiating contaminant oxidation. Hole oxidation could be the rate limiting step of phenol or atrazine degradation on both undoped and C-doped g-C₃N₄ in photocatalysis. Hole oxidation may produce a radical form of the contaminant, and the contaminant radical

Table 1 Summary of reactive species concentrations generated by undoped and C-doped g- G_3N_4 (U and $MCB_{0.07}$), second-order reaction rate constants of reactive species and contaminants, and measured pseudo-first-order reaction rate constants of contaminants degradation on the undoped and C-doped g- G_3N_4 .

			-	-		
	Sample	³ g-C ₃ N ₄ * ^a	·OH ^a	O2 ⁻ · a	¹ O ₂ ^a	H ₂ O ₂ ^b
Concentration of reactive species (M ⁻¹)	C-doped g-C ₃ N ₄	< 10 ^{-16 c}		9.6 (\pm 3.4) $\times 10^{-12}$	4.7 (± 2.0) ×10 ⁻¹²	3.1 (± 0.1) ×10 ⁻⁶
	Undoped g-C ₃ N ₄	$< 10^{-16} c$	$< 10^{-15} c$	$4.0 \ (\pm 0.6) \times 10^{-12}$	$2.4 (\pm 0.3)$ $\times 10^{-12}$	$2.0 (\pm 0.4) \times 10^{-6}$
k ₂ , second-order reaction rate constant	Atrazine/reactive species	$1.2 \times 10^{9} ^{d}$	2.5×10^9	10 ^{3 e}	$2.0 imes 10^5$	N.R. ^f
$(M^{-1} s^{-1})$	Phenol/reactive species	1.3×10^{3} d	1.4×10^{10}	5.8×10^2	2.6×10^6	N.R. ^f
k_{obs} , measured pseudo-first-order reaction rate constant (s ⁻¹)	Atrazine/C-doped g- C ₃ N ₄	8.0 (± 0.4)	× 10 ⁻⁴	Atrazine/undoped g- C ₃ N ₄	$1.0 \ (\pm 0.1) \times 10^{-4}$	
	Phenol/C-doped g- C ₃ N ₄	4.5 (± 0.2)	× 10 ⁻⁴	Phenol/undoped g- C ₃ N ₄	$4.0 \ (\pm 0.1) \times 10^{-4}$	

a Steady-state concentration.

b The concentration after a 6 h experiment.

c Less than the detection limit.

d Reaction rate constants approximated from those of the contaminants and triplet-excited state dissolved organic matter (3DOM*).

^e No literature data available, and the estimated value is less than or in the range of 10³ M⁻¹ s⁻¹.

 $^{^{\}mathrm{f}}$ No reaction (N.R.) between $\mathrm{H_{2}O_{2}}$ and atrazine or phenol.

could further react with the ROS produced in photocatalysis or O_2 at a much faster rate compared to the initial step of hole oxidation. To understand the mechanism and contribution of hole oxidation for contaminant transformation, we employed molecular simulations to interrogate the hole-contaminant interactions on both undoped and C-doped g-C₃N₄.

3.3. Simulations for hole oxidation of contaminants in photocatalysis

Two important processes in hole oxidation of the contaminants determine the overall reaction kinetics: the adsorption of contaminants on the g-C₃N₄ surface and electron transfer from the contaminants to the photo-excited g-C₃N₄. In our simulations, two contaminants, namely phenol and atrazine, and two types of g-C₃N₄, namely undoped and C-doped g-C₃N₄, were explored. Specifically, C-doped g-C₃N₄, where N atoms in the material are replaced by C atoms, may consist of two thermodynamically stable structures: N₁C-doped and N₃C-doped g-C₃N₄ (N₁C or N₃C represents C dopant in the N₁ or N₃ site, details of molecular structures are in Fig. S2) [13]. To ensure the accuracy and feasibility of the simulations, our simulation system consists of a bare, N₁C-doped, or N₃C-doped g-C₃N₄ single layer sheet, a contaminant, and typically ~3300 water molecules for full hydration to best represent our experimental conditions. In addition, the g-C₃N₄ sheet comprises 6×6 heptazine repeat units, with a dimension of 43.028 Å \times 43.028 Å (Fig. S3).

MD simulations were conducted to determining the adsorption of contaminants onto the g- C_3N_4 surface. The binding energy, E_b , is defined as the gap between the global minimum and the inner most peak of a free-energy surface. It thus decides the retention ratio upon adsorption, R_r, of a contaminant on a g-C₃N₄ sheet through the Boltzmann distribution: $R_T \propto e^{E_b/k_BT}$. The binding energy curves are presented in Fig. 1. In light of the notable hydrophilicity of the bare, undoped g-C₃N₄ sheet, it is not surprising to reveal a rather large E_h of 1.52 kcal mol⁻ for phenol, which is likewise hydrophilic (Fig. 1a). As for the hydrophobic atrazine, its E_h is substantially reduced to 0.68 kcal mol⁻¹ while its optimal binding distance to the g-C₃N₄ sheet is also shifted from 3.0 to 3.7 Å to reflect the expansion of molecular size (Fig. 1b). Interestingly, when an N₁C-doped g-C₃N₄ sheet with a dopant concentration of 11.1% is used (i.e. one N atom out of nine heptazine repeat units is doped by one C atom, raising the theoretical mass percent of carbon from 39.1% to 39.9%), atrazine exhibits an enhanced E_b of 0.90 kcal mol⁻¹, which is even greater than that of phenol by 0.36 kcal mol⁻¹ (Fig. 1b). The reversal of surface affinity can be ascribed to drastically reduced $\pi \to \pi$ stacking between the planar phenol molecule and the slightly corrugated N₁C-doped g-C₃N₄ sheet, whose enhanced hydrophobicity also facilities the retention of the hydrophobic atrazine. A similar trend was also observed on an N₃C-doped g-C₃N₄ sheet wherein atrazine has a stronger binding affinity than phenol by 0.23 kcal mol⁻¹ (Fig. 1c) when the same dopant concentration of 11.1% is applied.

Once a contaminant in the aqueous solution is adsorbed onto a g-C₂N₄ sheet, photo-induced interfacial electron transfer may take place in the presence of a favorable energy level alignment. For phenol and atrazine, their highest occupied molecular orbitals (HOMO) both lie between the valence band (VB) and the conduction band (CB) of the undoped and C-doped g-C₃N₄ sheets, making the direct oxidation of contaminants energetically feasible. The exothermicity of the photocatalytic oxidation can be further enhanced by the concerted proton transfer from these two contaminants, who both bear labile hydrogen atoms, to their nearest water molecules. For instance, the loss of the hydroxyl hydrogen atom in an oxidized phenol molecule to form a wellsolvated hydronium (Fig. 2a) would greatly stabilize the phenol/g-C₃N₄ adduct through charge neutralization and electrostatic screening. According to the Marcus non-adiabatic transition theory [43] extended for treating multiple reaction coordinates by including electron transfer, proton shuttling and solvent reorganization, the concerted proton-

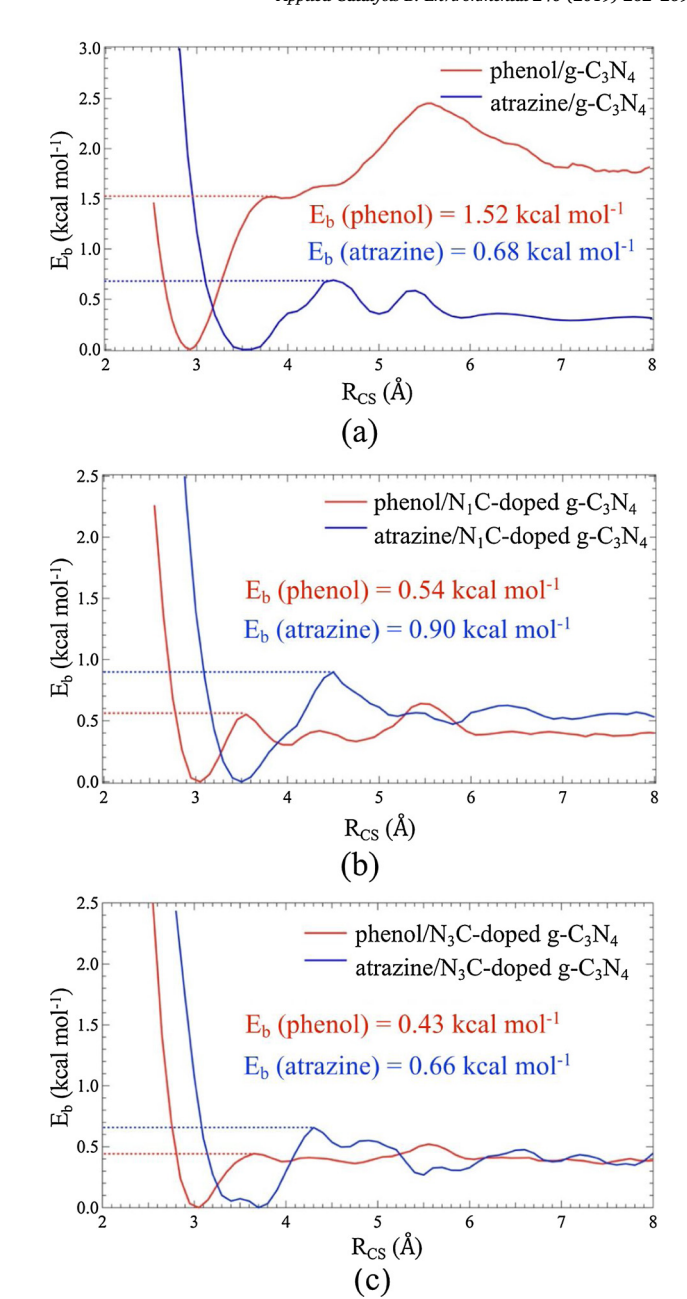


Fig. 1. Calculated binding free energy (E_b) profile of phenol and atrazine on undoped (a), N_1C -doped (b), and N_3C -doped (c) g- C_3N_4 sheets, respectively. The distance from the center of mass (COM) of the contaminant to the g- C_3N_4 sheet along its surface normal is defined as the reaction coordinate, R_{cs} , for their binding affinity.

coupled electron transfer (CPCET) rate [45], k_{CPCET} , is given by

$$k_{CPCET} = \sum_{\mu} P_{\mu} \sum_{\nu} \frac{J_{\mu\nu}^{2} \Xi_{\mu\nu}^{2}}{\hbar} \sqrt{\frac{\pi}{\lambda_{\mu\nu} k_{B} T}} e^{-\frac{(\Delta G_{\mu\nu}^{0} + \lambda_{\mu\nu})^{2}}{4\lambda_{\mu\nu} k_{B} T}}$$
(2)

where P_{μ} is the Boltzmann distribution of the μ -th reactant vibronic state, $J_{\mu\nu}$ is its electronic coupling strength with the ν -th product vibronic state, $\Xi_{\mu\nu}$ is the corresponding vibrational wavefunction overlap of proton shuttling, $\lambda_{\mu\nu}$ and $\Delta G_{\mu\nu}^0$ are the associated reorganization energy and driving force for the $\mu \to \nu$ transition, \hbar is the Planck constant $(6.63 \times 10^{-34} \ J \ s)$, k_B is the Boltzmann constant $(1.38 \times 10^{-23} \ J \ K^{-1})$, and T is the reaction temperature (298 K), respectively. Since the reaction coordinate of a CPCET process is typically dominated by the asymmetric stretching mode involving the transferring proton and its

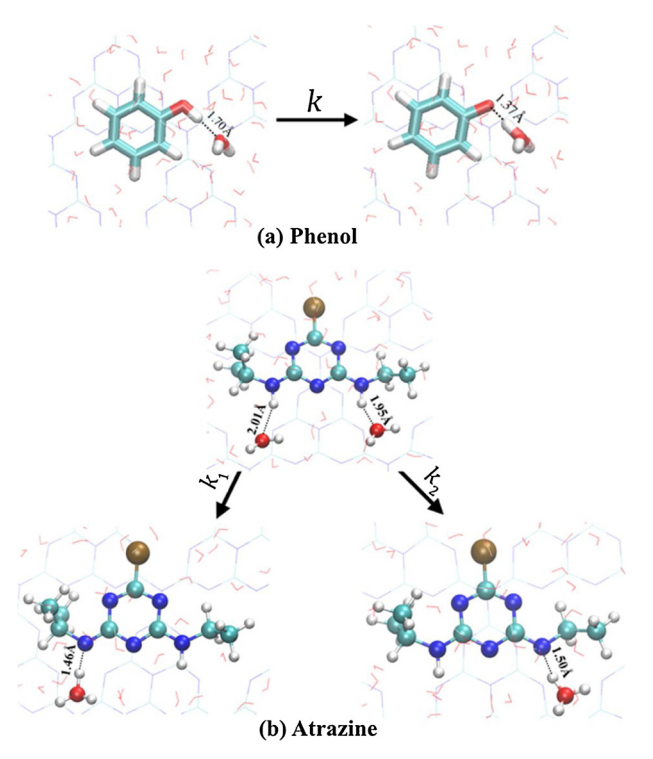


Fig. 2. Proposed concerted proton-coupled electron transfer (CPCET) reaction pathways for the photo-oxidation of phenol (a) and atrazine (b). The hydrogen, carbon, oxygen, nitrogen, and chlorine atom are labeled by white, cyan, red, blue, and brown color, respectively. (For interpretation of the references to colour in this figure legend, the reader is referred to the web version of this article).

two acceptors, the proton shuttling is expected to outpace the thermal fluctuation at room temperature, i.e., h $\omega_{CPCET} \approx 3000\,cm^{-1} \gg k_B\,T \approx 200\,cm^{-1}$. Therefore, only the ground reactant and product vibronic states ($\mu=0$ and $\nu=0$) are thermodynamically accessible, leading to a simplified CPCET rate:

$$k_{CPCET} \approx \frac{J_{00}^2 \Xi_{00}^2}{\hbar} \sqrt{\frac{\pi}{\lambda_{00} k_B T}} e^{-\frac{(\Delta G_{00}^0 + \lambda_{00})^2}{4 \lambda_{00} k_B T}} = \frac{J^2 \Xi^2}{\hbar} \sqrt{\frac{\pi}{\lambda k_B T}} e^{-\frac{(\Delta G^0 + \lambda)^2}{4 \lambda k_B T}}$$
(3)

where Ξ can be estimated by an overlap between two displaced Gaussian functions whose peaks are separated by the proton migration distance, Δ_P , along the CPCET reaction coordinate with an effective vibrational frequency of ω_P :

$$\Xi = \sqrt{\frac{m_P \omega_P}{\hbar \pi}} \int_{-\infty}^{\infty} dx e^{-\frac{x^2 m_P \omega_P}{2\hbar}} e^{-\frac{(x + \Delta x_P)^2 m_P \omega_P}{2\hbar}}$$
(4)

where m_P is the mass of proton (1.67 \times 10⁻²⁷ kg), and ω_P is determined from the energy gradient along the reaction coordinate. In addition, J was calculated by the constrained density functional theory [54], which was also employed to optimize the reactant and product states that are needed to evaluate ΔG^0 and λ according to our previously developed simulation protocol [55]. For instance, $\Delta G^0 = E_P - (E_{opt} + E_R)$, where E_P and E_R are the energies of the optimized product and reactant, respectively, and E_{opt} is the optical band gap at the optimized reactant structure. Note that the hydronium was constructed by imposing a collective hydrogen coordination number n_H of 3 for a central oxygen atom [56].

For our six contaminant/g- C_3N_4 adduct systems of interest, their key parameters to the photo-induced CPECT rate are summarized in Table 2. Specifically, all parameters were calculated using Goedecker-Tetter-Hutter (GTH) pseudopotential [57], Pedrew-Burke-Ernzehof hybrid (PBE0) exchange-correlation functional [58], polarized-valence-double- ζ (PVDZ) basis set [59], and density-derived atomic point

charges (DDAPC) [60]. Since atrazine has two secondary amine groups each consisting of a N-H bond as proton donor, the overall k_{CPCET} is thus a collective contribution from both reaction pathways (Fig. 2b). Nevertheless, the two N-H bonds are nearly chemically identical as illustrated by the notable similarity between their key parameters to k_{CPCET} . Upon the N₁C doping, k_{CPCET} for atrazine is almost unchanged (4.3 vs. $4.2\,\text{ns}^{-1}$ for undoped and $N_1\text{C-doped}$ g-C₃N₄), whereas it moderately drops to 1.2 ns⁻¹ when N₃C doping is adopted. The insensitivity of atrazine photo-oxidation to the g-C₃N₄ doping can be partially ascribed to their weaker $\pi \to \pi$ stacking due to the presence of atrazine's bulky and hydrophobic ethylamino and isopropylamino functional groups. Therefore, atrazine can tolerate or even appreciate a slightly corrugated aromatic sheet as also evidenced by its stronger E_h of 0.90 kcal mol⁻¹ to the N₁C-doped g-C₃N₄ when compared to 0.68 kcal mol⁻¹ for the undoped sheet. Unlike atrazine, phenol's coupling with a g-C₃N₄ sheet is very delicate to the surface roughness. For the planar undoped g-C₃N₄, the likewise planar phenol not only achieves a pronounced E_b of 1.52 kcal mol⁻¹, but also scores a rather compelling J of 76.5 meV. It is not surprising that J decays to 29.4 meV for the less planar N₁C-doped g-C₃N₄, and further to 14.2 meV for the most corrugated N₃C-dope g-C₃N₄. The deterioration of J is consistent with the reduced phenol/g-C₃N₄ contact area, which is desired by $\pi \to \pi$ stacking. Therefore, the introduction of C dopant into g-C₃N₄ decreases k_{CPCET} for phenol degradation, from 64.00 ns⁻¹ for undoped $g-C_3N_4$ to 27.70 and 3.20 ns⁻¹ for N_1C - and N_3C doped $g-C_3N_4$, respectively. Interestingly, the excellent alignment between ΔG_0 and λ for phenol oxidation is not altered upon doping, preserving the reaction in the Marcus barrierless region that results in a significantly greater k_{CPCET} than its counterpart for atrazine oxidation.

In our previous study, a small energy gap of 0.26 eV was found between the optimized N₁C- and N₃C-doped g-C₃N₄ sheets, suggesting the feasibility of their co-existence under experimental conditions [13]. However, in a doped g-C₃N₄ sheet, its undoped and doped heptazine repeat units may exhibit distinct propensities to anchor a near-surface contaminant. Since the two-dimensional translational symmetry of a g-C₃N₄ sheet is broken by the presence of doping sites, photo-generated excitons are most likely to be trapped there [13]. With regard to the spontaneous localization of excitons and thus their limited lifetime in doped g-C₃N₄, the proximity of a contaminant molecule to a doping site is critical to the photo-induced charge transfer between them. The proximity can be quantified by the relative propensity, which is obtained through projecting the COM of a contaminant onto its bound g-C₃N₄ sheet for all snapshots in a 1.0-ns molecular dynamics simulation trajectory before comparing the likelihoods of locating a projected COM onto doped and undoped heptazine repeat units. As shown in Table S2, both phenol and atrazine predominantly prefer an N₁C-doped heptazine unit over an N₃C-doped one as their binding site, making N₁C a much more effective doping scheme than N₃C. In other words, our calculated k_{CPCET} s for N₁C-doped g-C₃N₄ sheets should be much more relevant than the others when compared to experimental findings. As a rough guideline, the N₁C doping scheme is expected to facilitate the photooxidation of atrazine through enhanced contaminant adsorption (Fig. S2), whereas its efficacy on phenol oxidation would be attenuated due to the less-than-unity relative binding propensity (Table S2).

Based on the adsorption of contaminants $g\text{-}C_3N_4$ sheets and their CPCET reaction kinetics, we can conclude that C-doping favors the hole oxidation of atrazine but not of phenol. N_1C compared to N_3C sites contribute more significantly to the hole oxidation of the contaminants, due to its stronger interactions with the contaminants. Atrazine tends to bind more strongly onto the N_1C sites, and the CPCET reaction kinetics does not change upon doping. Nevertheless, phenol tends to move away from the C-doped sites, regardless of the doping scheme, and the binding energy to the C-doped sites is lower than that to the undoped ones. Moreover, C-dopants also reduce phenol degradation kinetics based on the CPCET mechanism. The simulations results are in agreement with our experimental observation, where atrazine degradation

Table 2 Key parameters for the evaluation of k_{CPCET} for contaminant/g-C₃N₄ adducts.

Adduct		$\Delta G_0(eV)$	a	$\lambda(eV)^{-1}$	b	J(meV)	c	$\Delta x_P(\text{Å})$	d	$\omega_P (cm^{-1}$) e	$E_{opt}(eV)$ f	$k_{CPCET} (ns^{-1})$ g
Phenol	Undoped g-C ₃ N ₄	-1.06		1.01		76.50		0.40		3151		2.75	64.00
	N ₁ C-doped g-C ₃ N ₄	-1.11		1.12		29.40		0.37		3126		2.57	27.70
	N ₃ C-doped g-C ₃ N ₄	-1.19		1.16		14.20		0.39		3137		2.94	3.20
Atrazine	Undoped g-C ₃ N ₄	-0.87	-0.77	0.66	0.55	47.10	63.80	0.44	0.48	3199	3140	2.75	4.30
	N ₁ C-doped g-C ₃ N ₄	-0.57	-0.48	0.74	0.66	41.10	40.10	0.44	0.46	3194	3199	2.57	4.20
	N ₃ C-doped g-C ₃ N ₄	-1.08	-0.96	0.71	0.60	59.50	54.80	0.45	0.48	3178	3162	2.94	1.20

^a ΔG^0 is the driving force of the CPCET process for the contaminant oxidation catalyzed by a photo-excited g-C₃N₄ sheet. $\Delta G^0 = E_P - (E_{opt} + E_R)$, where E_P and E_R are the energies of the optimized product and reactant, respectively, and E_{opt} is the optical band gap at the optimized reactant structure.

kinetics in photocatalysis was significantly improved after C-doping. Interestingly, the photodegradation kinetics of phenol did not decrease upon C-doping in our experiments. This discrepancy could be related with the low C-doping level in our fabricated sample or different surface areas of the undoped and C-doped g-C₃N₄. On one hand, as indicated in the simulations, phenol has a higher relative propensity binding to the undoped sites, and hence phenol reacts preferentially on the undoped sites. A low C-doping level would allow sufficient undoped sites for the phenol to reside and react on, and the reaction kinetics should be similar for undoped and C-doped g-C₃N₄. On the other hand, the C-doped g-C₃N₄ has a larger surface area than the undoped g-C₃N₄ (52.2 vs. 83.3 m² g⁻¹), which is expected to promote photocatalytic kinetics through providing more reaction sites and improving charge separation [13]. Similar reaction kinetics for both undoped and doped sample might suggest C-dopant inhibits intrinsic reactivity for phenol oxidation. Most importantly, it is worth noting that k_{CPCET} only presents the rate of single-electron transfer from adsorbed contaminants to the photo-excited g-C₃N₄, and thus it cannot be quantitatively translated into the contaminant degradation rate constant observed in our previous study. Many other complex processes, experimental conditions, and photocatalyst properties also affect the measured reaction rate constant in photocatalysis, such as photocatalyst absorption of photons, charge separation rate, electron-hole recombination rate, back-reaction of the contaminant radical and the ground-state g-C₃N₄, and these factors were not included in the simulations. Even though the simulations cannot quantitatively reflect the observed contaminant oxidation rates in experiments, for the first time, the results highlight the significant role of C-dopant in g-C₃N₄ to the hole oxidation of contaminants.

3.4. Mechanism and implication

By taking the advantage of the synergy of experimental quantifications and computational simulations, we elucidate the mechanism of contaminant photocatalytic degradation on visible-light-responsive g- C_3N_4 . Both undoped and C-doped g- C_3N_4 did not generate an observable amount of $\cdot OH$ or 3g - C_3N_4* , and these two samples produced $O_2^{-}\cdot,\ ^1O_2$, and H_2O_2 as the ROS in photocatalysis. However, the selected organic contaminants in our study, i.e., phenol and atrazine, do not react at all or react with these ROS slowly. Hole oxidation is believed to determine the overall kinetics of contaminant degradation, whereas both contaminant adsorption onto the photocatalyst and direct

electron transfer from the contaminant to the photo-excited photo-catalyst via the CPCET process are important. Molecular simulations elucidate that C-doping promotes the hole oxidation of atrazine whereas inhibits the hole oxidation of phenol compared to undoped g- C_3N_4 . We speculate that the contaminants generate their radical forms via hole oxidation first, which is the rate determining step, and the radicals further reacts with ROS or O_2 to form stable daughter products.

Our work highlights the significant role of hole oxidation in photocatalysis for contaminant transformation for the first time, via a rigorous experimental and simulation approach. For Many UV-light-responsive photocatalysts, such as TiO2 and ZnO, ·OH played a dominant role in contaminant transformation, and the reactions between ·OH and a broad suite of contaminants were well-documented. For many visiblelight-responsive photocatalysts, not limited to g-C₃N₄, their valence band edges are not sufficiently positive to oxidize water and produce a large amount of ·OH, and therefore other ROS or even the holes determine the overall reaction kinetics. Very few study focused on the hole oxidation, and the role for chemical transformation was largely unknown. Scavenger tests, with the addition of a chemical to quench the reaction between the scavenger and the reactive species selectively, were adopted to quantify the contribution of the ROS or the holes for contaminant degradation. However, the results of the scavenger tests should be scrutinized because the reaction selectivity could be compromised in photocatalysis (especially OH and the holes may potentially oxidize many scavengers) and thus there are artifacts for result interpretation [14]. For future studies, more experimental and theoretical work should be conducted for photocatalysis to quantify the holes and understand hole-contaminant interactions.

The important application of this study is to guide rational material design for contaminant removal in photocatalysis. As we now understand the critical role of the holes for contaminant transformation, material design that enhances contaminant adsorption to the photocatalyst, charge separation, surface areas, and photon adsorption should be considered. More importantly, hole oxidation of contaminants is a highly selective process, and it opens a new avenue for contaminant degradation in complex water matrices. One significant limitation of ROS-driven photocatalysis is notably inhibited reactivity with the presence of water constituents. For example, ·OH oxidation for contaminant removal suffers greatly with the presence of carbonate or natural organic matter (NOM), because these species may compete with the contaminants of much lower concentrations for ·OH in reactions [61–63], or form less reactive species (CO_3 · $^-$) that lowers contaminant

 $^{^{\}mathrm{b}}$ λ is the reorganization energy associated with the CPCET process.

^c *J* is electronic coupling strength between the reactant and product of the CPCET process.

^d Δ_P is the distance of proton migration.

^e ω_P is the angular frequency of proton shuttling.

^f E_{opt} is the optical band gap of g-C₃N₄.

 $^{^{\}rm g}~k_{CPCET}$ is the CPCET reaction rate.

degradation kinetics. ¹O₂ oxidation for contaminants is also inhibited in complex water matrices, though to a less extent than ·OH [64]. Our previous study observed little to no inhibition for atrazine degradation on the C-doped g-C₃N₄ with the presence of simulated complex water matrices and (partially) treated drinking water and wastewater in photocatalysis [13]. The robustness of the photocatalyst for contaminant degradation could be attributed to selective hole oxidation of the contaminant. C-dopant promotes the binding between atrazine and the photocatalyst and maintain the CPCET reactivity compared to the undoped counterpart, whereas the other water constituents may not be as competitive as atrazine on g-C₃N₄ in photocatalytic oxidation. The selective hole oxidation could also have a huge impact in chemical synthesis by photocatalysis, e.g., pharmaceuticals, phenol (from benzene oxidation). Compared to conventional methods to produce these chemicals, selective photocatalysis could increase the yield of desired products, reduce the cost and chemical/energy footprint, and promote green chemistry and sustainability.

4. Conclusion

In this study, we elucidated the mechanism of contaminant transformation on visible-light-responsive g-C₃N₄ in photocatalysis, and highlighted the critical role of the holes for contaminant oxidation via a synergistic experimental and simulation approach for the first time. For both undoped and C-doped g-C₃N₄, hole oxidation determined the reaction kinetics of the contaminants, in contrast to the other reactive species, including ROS (i.e., ·OH, O2 -·/HO2·, ¹O2, H2O2) and tripletexcited states (³g-C₃N₄*). MD and DFT simulations were used to explore the adsorption of the contaminants on the photocatalyst surface and electron transfer kinetics from the contaminants to the excited photocatalysts, which are two critical processes in the hole oxidation. Cdoping significantly enhanced the binding affinity of atrazine on g-C₃N₄ but reduced that of phenol on g-C₃N₄. C-doping reduced the CPECT rate of phenol on g-C₃N₄, but did not affect that of atrazine. These results could explain the selective oxidation of phenol and atrazine on undoped and C-doped g-C₃N₄ observed in our previous study. The exploration of contaminant transformation mechanism, especially hole oxidation, fills in the gap of our understanding of visible-light-responsive photocatalysis. The research outcome will promote the rational and smart design of g-C₃N₄ for applications with enhanced selectivity, including contaminant degradation, chemical synthesis, and beyond.

Acknowledgements

We acknowledgethe NSF Grant CBET-1437989, USDA-NIFA Grant 2017-67021-26602, and GW Columbian College Facilitating Fund for supporting our study. Computational resources were provided under DOE contract DE-AC02-06CH11357 and NSF contract TG-CHE130008. E. Park appreciates the support from Madeleine Reines Jacobs undergraduate research fellowship of GW Chemistry Department.

Appendix A. Supplementary data

Supplementary material related to this article can be found, in the online version, at doi:https://doi.org/10.1016/j.apcatb.2018.09.012.

References

- [1] M. Long, W. Cai, J. Cai, B. Zhou, X. Chai, Y. Wu, Efficient photocatalytic degradation of phenol over Co₃O₄/BiVO₄ composite under visible light irradiation, J. Phys. Chem. B 110 (2006) 20211–20216.
- [2] X. Wang, K. Maeda, A. Thomas, K. Takanabe, G. Xin, J.M. Carlsson, K. Domen, M. Antonietti, A metal-free polymeric photocatalyst for hydrogen production from water under visible light, Nat. Mater. 8 (2009) 76–80.
- [3] H. Wang, Y. Su, H. Zhao, H. Yu, S. Chen, Y. Zhang, X. Quan, Photocatalytic oxidation of aqueous ammonia using atomic single layer graphitic-C₃N₄, Environ. Sci. Technol. 48 (2014) 11984–11990.
- [4] M.N. Chong, B. Jin, C.W.K. Chow, C. Saint, Recent developments in photocatalytic

- water treatment technology: a review, Water Res. 44 (2010) 2997-3027.
- [5] D.B. Hernández-Uresti, A. Vázquez, D. Sanchez-Martinez, S. Obregón, Performance of the polymeric g-C₃N₄ photocatalyst through the degradation of pharmaceutical pollutants under UV-vis irradiation, J. Photochem. Photobiol. A: Chem. 324 (2016) 47–52.
- [6] Y. Hong, Y. Jiang, C. Li, W. Fan, X. Yan, M. Yan, W. Shi, In-situ synthesis of direct solid-state Z-scheme V₂O₅/g-C₃N₄ heterojunctions with enhanced visible light efficiency in photocatalytic degradation of pollutants, Appl. Catal. B 180 (2016) 663-673
- [7] H. Liu, Z. Jin, Z. Xu, Z. Zhang, D. Ao, Fabrication of ZnIn₂S₄-g-C₃N₄ sheet-on-sheet nanocomposites for efficient visible-light photocatalytic H₂-evolution and degradation of organic pollutants, RSC Adv. 5 (2015) 97951–97961.
- [8] Z. Zhu, X. Tang, C. Ma, M. Song, N. Gao, Y. Wang, P. Huo, Z. Lu, Y. Yan, Fabrication of conductive and high-dispersed Ppy@Ag/g-C₃N₄ composite photocatalysts for removing various pollutants in water, Appl. Surf. Sci. 387 (2016) 366–374.
- [9] K. Li, Z. Zeng, L. Yan, M. Huo, Y. Guo, S. Luo, X. Luo, Fabrication of C/X-TiO₂@C₃N₄, NTs (X=N, F, Cl) composites by using phenolic organic pollutants as raw materials and their visible-light photocatalytic performance in different photocatalytic systems, Appl. Catal. B 187 (2016) 269–280.
- [10] G. Dong, Z. Ai, L. Zhang, Efficient anoxic pollutant removal with oxygen functionalized graphitic carbon nitride under visible light, RSC Adv. 4 (2014) 5553–5560.
- [11] Y. Hong, C. Li, G. Zhang, Y. Meng, B. Yin, Y. Zhao, W. Shi, Efficient and stable Nb₂O₅ modified g-C₃N₄ photocatalyst for removal of antibiotic pollutant, Chem. Eng. J. 299 (2016) 74–84.
- [12] W.-J. Ong, L.-L. Tan, Y.H. Ng, S.-T. Yong, S.-P. Chai, Graphitic carbon nitride (g-C₃N₄)-based photocatalysts for artificial photosynthesis and environmental remediation: are we a step closer to achieving sustainability? Chem. Rev. 116 (2016) 7159–7329.
- [13] Q. Zheng, D.P. Durkin, J.E. Elenewski, Y. Sun, N.A. Banek, L. Hua, H. Chen, M.J. Wagner, W. Zhang, D. Shuai, Visible-light-responsive graphitic carbon nitride: rational design and photocatalytic applications for water treatment, Environ. Sci. Technol. 50 (2016) 12938–12948.
- [14] Q. Zheng, H. Shen, D. Shuai, Emerging investigators series: advances and challenges of graphitic carbon nitride as a visible-light-responsive photocatalyst for sustainable water purification, Environ. Sci.: Water Res. Technol. 3 (2017) 982–1001.
- [15] K.M. Lee, C.W. Lai, K.S. Ngai, J.C. Juan, Recent developments of zinc oxide based photocatalyst in water treatment technology: a review, Water Res. 88 (2016) 428–448
- [16] J. Staehelin, J. Hoigne, Decomposition of ozone in water in the presence of organic solutes acting as promoters and inhibitors of radical chain reactions, Environ. Sci. Technol. 19 (1985) 1206–1213.
- [17] P. Fernández-Castro, M. Vallejo, M.F.S. Román, I. Ortiz, Insight on the fundamentals of advanced oxidation processes. Role and review of the determination methods of reactive oxygen species, J. Chem. Technol. Biotechnol. 90 (2015) 796–820.
- [18] J.M. Burns, W.J. Cooper, J.L. Ferry, D.W. King, B.P. DiMento, K. McNeill, C.J. Miller, W.L. Miller, B.M. Peake, S.A. Rusak, A.L. Rose, T.D. Waite, Methods for reactive oxygen species (ROS) detection in aqueous environments, Aquat. Sci. 74 (2012) 683–734.
- [19] H. Wang, S. Jiang, S. Chen, X. Zhang, W. Shao, X. Sun, Z. Zhao, Q. Zhang, Y. Luo, Y. Xie, Insights into the excitonic processes in polymeric photocatalysts, Chem. Sci. 8 (2017) 4087–4092.
- [20] H. Wang, S. Jiang, S. Chen, D. Li, X. Zhang, W. Shao, X. Sun, J. Xie, Z. Zhao, Q. Zhang, Y. Tian, Y. Xie, Enhanced singlet oxygen generation in oxidized graphitic carbon nitride for organic synthesis, Adv. Mater. 28 (2016) 6940–6945.
- [21] F.L. Rosario-Ortiz, S. Canonica, Probe compounds to assess the photochemical activity of dissolved organic matter, Environ. Sci. Technol. 50 (2016) 12532–12547.
- [22] K. McNeill, S. Canonica, Triplet state dissolved organic matter in aquatic photochemistry: reaction mechanisms, substrate scope, and photophysical properties, Environ. Sci.: Processes Impacts. 18 (2016) 1381–1399.
- [23] M. Sun, Q. Yan, T. Yan, M. Li, D. Wei, Z. Wang, Q. Wei, B. Du, Facile fabrication of 3D flower-like heterostructured g-C₃N₄/SnS₂ composite with efficient photocatalytic activity under visible light, RSC Adv. 4 (2014) 31019–31027.
- [24] D. Ma, A. Liu, C. Lu, C. Chen, Photocatalytic dehydrogenation of primary alcohols: selectivity goes against adsorptivity, ACS Omega 2 (2017) 4161–4172.
- [25] Y. Tamaki, A. Furube, M. Murai, K. Hara, R. Katoh, M. Tachiya, Direct observation of reactive trapped holes in TiO₂ undergoing photocatalytic oxidation of adsorbed alcohols: evaluation of the reaction rates and yields, J. Am. Chem. Soc. 128 (2006) 416, 417.
- [26] J.B. Sambur, P. Chen, Distinguishing direct and indirect photoelectrocatalytic oxidation mechanisms using quantitative single-molecule reaction imaging and photocurrent measurements, J. Phys. Chem. C. 120 (2016) 20668–20676.
- [27] F. De Angelis, A. Tilocca, A. Selloni, Time-dependent DFT study of ${\rm [Fe(CN)_6]}^4$ sensitization of TiO₂ nanoparticles, J. Am. Chem. Soc. 126 (2004) 15024–15025.
- [28] M. Pastore, F.D. Angelis, Computational modelling of TiO₂ surfaces sensitized by organic dyes with different anchoring groups: Adsorption modes, electronic structure and implication for electron injection/recombination, Phys. Chem. Chem. Phys. 14 (2011) 920–928.
- [29] K. Lee, H. Ku, D. Pak, OH radical generation in a photocatalytic reactor using TiO₂ nanotube plates, Chemosphere. 149 (2016) 114–120.
- [30] M. Cho, H. Chung, W. Choi, J. Yoon, Linear correlation between inactivation of E. Coli and OH radical concentration in TiO₂ photocatalytic disinfection, Water Res. 38 (2004) 1069–1077.
- [31] C.-Y. Chen, C.T. Jafvert, Photoreactivity of carboxylated single-walled carbon nanotubes in sunlight: reactive oxygen species production in water, Environ. Sci. Technol. 44 (2010) 6674–6679.
- [32] S. Mostafa, F.L. Rosario-Ortiz, Singlet oxygen formation from wastewater organic

- matter, Environ. Sci. Technol. 47 (2013) 8179-8186.
- [33] X. Xu, X. Duan, Z. Yi, Z. Zhou, X. Fan, Y. Wang, Photocatalytic production of superoxide ion in the aqueous suspensions of two kinds of ZnO under simulated solar light, Catal. Commun. 12 (2010) 169–172.
- [34] H. Bader, V. Sturzenegger, J. Hoigné, Photometric method for the determination of low concentrations of hydrogen peroxide by the peroxidase catalyzed oxidation of N,N-diethyl-p-phenylenediamine (DPD), Water Res. 22 (1988) 1109–1115.
- [35] J.E. Grebel, J.J. Pignatello, W.A. Mitch, Sorbic acid as a quantitative probe for the formation, scavenging and steady-state concentrations of the triplet-excited state of organic compounds, Water Res. 45 (2011) 6535–6544.
- [36] G.M. Torrie, J.P. Valleau, Nonphysical sampling distributions in Monte Carlo freeenergy estimation: umbrella sampling, J. Comput. Phys. 23 (1977) 187–199.
- [37] S. Kumar, J.M. Rosenberg, D. Bouzida, R.H. Swendsen, P.A. Kollman, THE weighted histogram analysis method for free-energy calculations on biomolecules. I. The method, J. Comput. Chem. 13 (1992) 1011–1021.
- [38] J. Wang, R.M. Wolf, J.W. Caldwell, P.A. Kollman, D.A. Case, Development and testing of a general amber force field, J. Comput. Chem. 25 (2004) 1157–1174.
- [39] Y. Wu, H.L. Tepper, G.A. Voth, Flexible simple point-charge water model with improved liquid-state properties, J. Chem. Phys. 124 (2006) 024503.
- [40] S. Nosé, A unified formulation of the constant temperature molecular dynamics methods, J. Chem. Phys. 81 (1984) 511–519.
- [41] W.G. Hoover, Canonical dynamics: equilibrium phase-space distributions, Phys. Rev. A (Coll Park) 31 (1985) 1695–1697.
- [42] J. VandeVondele, M. Krack, F. Mohamed, M. Parrinello, T. Chassaing, J. Hutter, Quickstep: fast and accurate density functional calculations using a mixed Gaussian and plane waves approach, Comput. Phys. Commun. 167 (2005) 103–128.
- [43] R.A. Marcus, Electron transfer reactions in chemistry. Theory and experiment, Rev. Mod. Phys. 65 (1993) 599–610.
- [44] P.A.M. Dirac, The quantum theory of the emission and absorption of radiation, Proc. R. Soc. Lond. A. 114 (1927) 243–265.
- [45] S. Hammes-Schiffer, A.A. Stuchebrukhov, Theory of coupled electron and proton transfer reactions, Chem. Rev. 110 (2010) 6939–6960.
- [46] D. Xia, Z. Shen, G. Huang, W. Wang, J.C. Yu, P.K. Wong, Red phosphorus: an earth-abundant elemental photocatalyst for "green" bacterial inactivation under visible light, Environ. Sci. Technol. 49 (2015) 6264–6273.
- [47] B.H.J. Bielski, D.E. Cabelli, R.L. Arudi, A.B. Ross, Reactivity of HO₂/O₂⁻ radicals in aqueous solution, J. Phys. Chem. Ref. Data 14 (1985) 1041–1100.
- [48] T. Zeng, W.A. Arnold, Pesticide photolysis in prairie potholes: probing photosensitized processes, Environ. Sci. Technol. 47 (2013) 6735–6745.
- [49] National Institude of Standards and Technology, NDRL/NIST Solution Kinetics Database, (2018) (Accessed May 3, 2018), https://kinetics.nist.gov/solution/index.

- jsp.
- [50] T. Yasuhisa, H. Hideki, Y. Muneyoshi, Superoxide radical scavenging activity of phenolic compounds, Int. J. Biochem. Cell Biol. 25 (1993) 491–494.
- [51] M. Hayyan, M.A. Hashim, I.M. AlNashef, Superoxide ion: generation and chemical implications, Chem. Rev. 116 (2016) 3029–3085.
- [52] D.F. Ollis, Kinetic disguises in heterogeneous photocatalysis, Top. Catal. 35 (2005) 217–223
- [53] S. Canonica, U. Jans, K. Stemmler, J. Hoigne, Transformation kinetics of phenols in water: photosensitization by dissolved natural organic material and aromatic ketones, Environ. Sci. Technol. 29 (1995) 1822–1831.
- [54] Q. Wu, T. Van Voorhis, Extracting electron transfer coupling elements from constrained density functional theory, J. Chem. Phys. 125 (2006) 164105.
- [55] J.E. Elenewski, J.Y. Cai, W. Jiang, H. Chen, Functional mode hot electron transfer theory, J. Phys. Chem. C. 120 (2016) 20579–20587.
- [56] A. Hassanali, M.K. Prakash, H. Eshet, M. Parrinello, On the recombination of hydronium and hydroxide ions in water, PNAS. 108 (2011) 20410–20415.
- [57] S. Goedecker, M. Teter, J. Hutter, Separable dual space Gaussian pseudo-potentials, Phys. Rev. B 54 (1996) 1703–1710.
- [58] J.P. Perdew, M. Ernzerhof, K. Burke, Rationale for mixing exact exchange with density functional approximations, J. Chem. Phys. 105 (1996) 9982–9985.
- [59] D.E. Woon, T.H. Dunning, Gaussian basis sets for use in correlated molecular calculations. IV. Calculation of static electrical response properties, J. Chem. Phys. 100 (1994) 2975–2988.
- [60] P.E. Blöchl, Electrostatic decoupling of periodic images of plane-wave-expanded densities and derived atomic point charges, J. Chem. Phys. 103 (1995) 7422–7428.
- [61] M.G. Antoniou, C. Zhao, K.E. O'Shea, G. Zhang, D.D. Dionysiou, C. Zhao, C. Han, M.N. Nadagouda, H. Choi, T. Fotiou, T.M. Triantis, A. Hiskia, CHAPTER 1: photocatalytic degradation of organic contaminants in water: process optimization and degradation pathways, Photocatalysis, (2016), pp. 1–34.
- [62] J. Brame, M. Long, Q. Li, P. Alvarez, Trading oxidation power for efficiency: differential inhibition of photo-generated hydroxyl radicals versus singlet oxygen, Water Res. 60 (2014) 259–266.
- [63] J. Brame, M. Long, Q. Li, P. Alvarez, Inhibitory effect of natural organic matter or other background constituents on photocatalytic advanced oxidation processes: mechanistic model development and validation, Water Res. 84 (2015) 362–371.
- [64] H. Kim, W. Kim, Y. Mackeyev, G.-S. Lee, H.-J. Kim, T. Tachikawa, S. Hong, S. Lee, J. Kim, L.J. Wilson, T. Majima, P.J.J. Alvarez, W. Choi, J. Lee, Selective oxidative degradation of organic pollutants by singlet oxygen-mediated photosensitization: tin porphyrin versus C₆₀ aminofullerene systems, Environ. Sci. Technol. 46 (2012) 9606–9613.